Vector soliton and noise-like pulse generation using a Ti$_3$C$_2$ MXene material in a fiber laser[*]

Shuai WANG[1], Lei LI[†1], Yu-feng SONG[2], Ding-yuan TANG[3], De-yuan SHEN[1], Lu-ming ZHAO[†‡1,4]

[1]*Jiangsu Key Laboratory of Advanced Laser Materials and Devices, Jiangsu Collaborative Innovation Center of Advanced Laser Technology and Emerging Industry, School of Physics and Electronic Engineering, Jiangsu Normal University, Xuzhou 221116, China*

[2]*Shenzhen Engineering Laboratory of Phosphorene and Optoelectronics, International Institute of Microscale Optoelectronics, International Collaborative Laboratory of 2D Materials for Optoelectronics Science and Technology of Ministry of Education, Shenzhen University, Shenzhen 518060, China*

[3]*School of Electrical and Electronic Engineering, Nanyang Technological University, Singapore 639798, Singapore*

[4]*Kunshan Shunke Laser Technology Co., Ltd., Suzhou 215300, China*

[†]E-mail: sdulilei@gmail.com; lmzhao@ieee.org

Abstract: We built a Tm:Ho co-doped fiber laser using a Ti$_3$C$_2$ MXene material as a saturable absorber (SA). The formation of vector solitons (VSs) and noise-like pulses (NLPs) was observed. The SA was prepared by dripping a Ti$_3$C$_2$ solution on a side-polished D-shaped fiber and then naturally vaporized. The VS is characterized by two coexisting sets of Kelly sidebands. By modulating the polarization controller in the fiber laser, NLPs with about 3.3 nm bandwidth can be switched from the VS. To the best of our knowledge, this is the first time that VSs have been generated in a fiber laser using a Ti$_3$C$_2$ MXene material as the SA.

Key words: Vector soliton; Noise-like pulse; MXene; Laser fiber

https://doi.org/10.1631/FITEE.2000033 **CLC number:** TN29

1 Introduction

Fiber lasers are widely used in optical fiber communications, laser marking, laser cutting, military defense, and medical fields because of their compact structure, easier integration, and better beam quality as compared with other lasers (Shi et al., 2014). Mode-locked fiber lasers have attracted the attention of many researchers because of their capability of generating pulses with a narrow pulse width, high peak power, and abundant dynamic phenomena. Active mode-locking and passive mode-locking are the main techniques used to achieve mode-locking in a fiber laser. The widely used passive mode-locking method uses mainly a saturable absorber (SA) to narrow the pulse, and the SA is divided into a physical SA and an artificial SA. In recent years, various new materials have been used as physical SAs to achieve mode-locking in fiber lasers. Zhang H et al. (2009) showed that a single pulse energy of 7.3 nJ and a pulse width of 415 fs could be obtained by integrating the atomic layer graphene as a SA into an Er-doped passive mode-locked fiber laser. Nicholson et al. (2007) used a single-wall carbon nanotube (SWCNT) based SA to generate a mode-locked pulse with a pulse duration of 247 fs at a central wavelength of 1560 nm in an Er-doped fiber

---

laser. They also generated a mode-locked pulse with a pulse duration of 137 fs at a central wavelength of 1070 nm in an amplified Yb-doped fiber laser (Nicholson et al., 2007). By integrating a black phosphorus (BP) based SA into an Er-doped fiber laser, Chen et al. (2015) obtained Q-switching at a maximum pulse energy of 94.3 nJ and passive mode-locked pulses with a pulse width of 946 fs.

Including the above, two-dimensional (2D) materials have attracted extensive attention in materials science due to their excellent properties (Luo et al., 2010; Zhang H et al., 2010; Qin et al., 2015; Sotor et al., 2015; Song et al., 2016; Jiang T et al., 2020). In recent years, a new type of 2D material known as MXenes, which are composed of elements such as transition metal carbides, nitrides, and carbonitrides, have attracted the interest of researchers due to their good electrical conductivity, high elastic modulus, high capacitance, tunable band gap, and high optical transmission (Naguib et al., 2011; Lei et al., 2015). They also have excellent optical characteristics. In 2016, Gogotsi's team produced a transparent $Ti_3C_2T_x$ MXene film with optoelectronic tunable characteristics (Hantanasirisakul et al., 2016). Later, some researchers used Ti_3CNT_x and $Ti_3C_2T_x$ to achieve a femtosecond pulse mode-locked laser output in the visible and near-infrared wavelength ranges, thus proving the superior advantages of the MXene in broadband applications (Wang et al., 2018, 2019). Feng et al. (2018) used an MXene as a SA for the first time to achieve passive Q-switching at 1060 nm in a Nd:YAG ceramic laser. Subsequently, researchers achieved Q-switching and highly stable femtosecond pulse mode-locked fiber lasers in the near-infrared communication band to the shortwave infrared band using $Ti_3C_2T_x$ MXene as a SA (Wang et al., 2018; Li et al., 2019; Zu et al., 2019). It showed the broadband saturated absorption characteristics of this material and its applicability as a SA. Jiang Q et al. (2019) integrated a microfiber-based $Ti_3C_2T_x$ MXene SA to achieve soliton mode-locking with a pulse duration of 2.11 ps at 2 μm for the first time in a Tm-doped all-fiber laser. All of these results proved the superior advantages of an MXene SA in broadband applications. These optical characteristics indicate that it has a high research value in the field of fiber lasers. Moreover, the application potential of MXenes in the mid-infrared ultrafast fiber laser was proved. In

addition, the 2 μm wavelength region has great potential in the fields of light detection and ranging (LIDAR) and gas sensing. Due to the strong absorption of water in this band, the 2 μm laser has been widely used in medical fields (Scholle et al., 2010).

In this study, we achieved passive mode-locking by integrating a homemade Ti_3C_2 MXene SA into a Tm:Ho co-doped fiber laser. By adjusting the appropriate parameters in the cavity, we obtained an output of traditional vector solitons (VSs) and noise-like pulses (NLPs). The VS is characterized by two co-existing sets of Kelly sidebands, which is the overlap of the two polarization components. By modulating the polarization controller in the fiber laser, the NLPs of about 3.3 nm bandwidth can be switched from the VS. To the best of our knowledge, this is the first time that VSs have been generated in a fiber laser using the Ti_3C_2 MXene material as the SA.

2 Fabrication and properties of Ti_3C_2 MXene SA

The liquid acid etching exfoliation method is a common method for converting layered bulk materials into ultrathin 2D materials. The Ti_3C_2 MXene we used was fabricated by Song et al. (Song et al., 2019a; Wang et al., 2019), using the liquid acid etching exfoliation method. MXene nanosheets were dissolved into N-Methyl-2-pyrrolidone (NMP) at a concentration of 0.1 mg/mL and dispersed by ultrasonic bath (Fig. 1a). Fig. 1b shows a piece of the side-polished D-shaped fiber with a 6 μm polishing depth from the core, which was used to add the MXene SA into the fiber laser.

The D-shaped fiber we used was SMF-28e. Before the MXene was deposited on the D-shaped fiber to make an MXene SA, the polishing depth of the D-shaped fiber was measured with a microscope
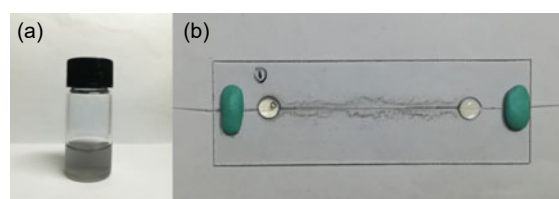

Fig. 1 Schematic of the Ti_3C_2 MXene solution (a) and homemade saturable absorber (SA) (b)

(Axio Scope.A1, ZEISS, Germany). The D-shaped fiber was placed on the glass slide, and we rotated the fiber so that the polishing plane was approximately perpendicular to the glass plane. Then, the depth-of-field expansion function of the microscope's camera was used to take measurements of the upper and lower boundaries (polished region) of the optical fiber. Fig. 2a is a schematic of polishing depth measurement. Fig. 2b is a D-shaped fiber photographed by the microscope. The upper edge is the edge of the fiber cladding and the lower edge is the polishing plane. The cladding diameter and core diameter of SMF-28e are 125 μm and 8 μm, respectively. Therefore, when the polishing depth is 6 μm, the distance

between the two boundaries measured with a microscope should be 72.5 μm (Fig. 2b). The mosaic-like part of the picture is the normal phenomenon after the picture was processed with a computer. The MXene material was attached to the side-polished area after dripping the MXene solution onto the D-shaped fiber with a needle. After being naturally vaporized, the Ti_3C_2 MXene would interact with the intracavity light through the evanescent field to achieve the role of a SA.

A nonlinear polarization rotation (NPR) passively mode-locked fiber laser was set up as a seed to measure the saturable absorption characteristics of the MXene SA that we prepared. By properly adjusting the polarization controller, it can work in a stable soliton mode-locked state with a center wavelength of 1958 nm and a repetition rate of 13.23 MHz. Using this fiber laser source as a seed, the saturable absorption of the MXene SA was measured (Fig. 3). The transmission gradually increased as the incident optical power into the SA increased. However, due to the low peak power of the pulse, the saturation region was not approached. The fitting saturable absorber model is given by the following equation (Lu et al., 2017):

$$T(I) = 1 - \varphi_0 \exp(-I / I_{sat}) - \varphi_{ns}, \tag{1}$$

where $T(I)$ is the transmittance, φ_0 the modulation depth, I_{sat} the saturation optical intensity, I the incident optical intensity, and φ_{ns} the nonsaturable loss. It can be seen from the results that the modulation depth of the saturable absorber is 2.1%.
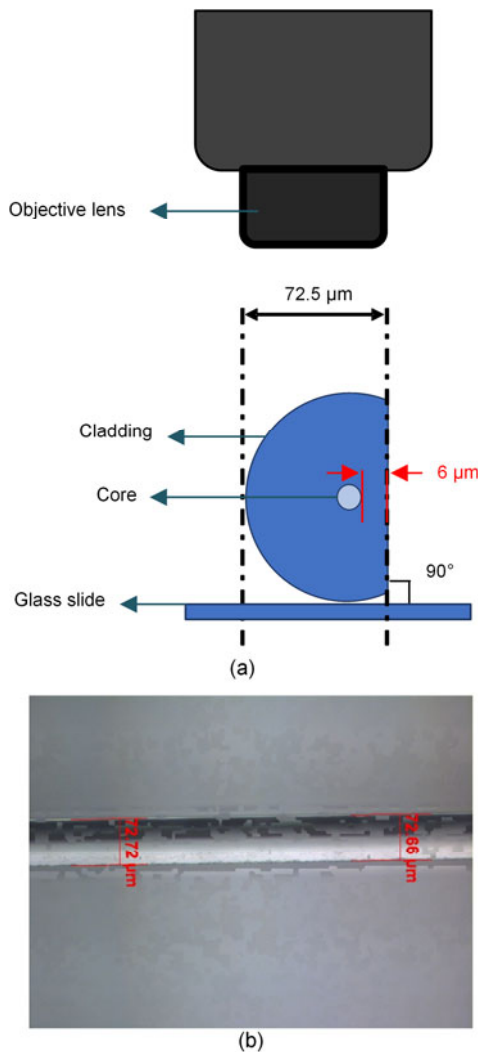

Fig. 2 Schematic of polishing depth measurement (a) and D-shaped fiber photographed by the depth-of-field extension function of the microscope (b)
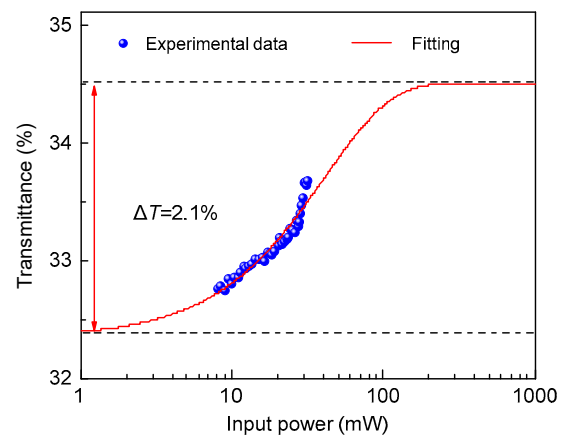

Fig. 3 Nonlinear saturable absorption of the Ti_3C_2 MXene saturable absorber (SA)

3 Experimental setup

The schematic of the fiber laser system is shown in Fig. 4. The laser cavity includes a side-polished D-shaped fiber (SMF) Ti_3C_2 saturable absorber, a 3 m Thulium/Holmium-doped fiber (TDF) (TH512, Cor-Active Inc., Canada), which is pumped by a 1550 nm benchtop amplification laser system (Connet MARS) through a wavelength division multiplexer (WDM), a polarization insensitive isolator with 0.9 dB insertion loss, and an isolation of greater than 18 dB at 2 μm wavelength which is spliced into the cavity to enforce a counterclockwise unidirectional ring. The total length of the Ti_3C_2 MXene SA including the pigtails is 2 m. The length is about 2 cm. The insertion loss of the MXene SA is about 9 dB. A paddle polarization controller and an in-line manual fiber polarization controller are used for more precise adjustment of the intracavity polarization state. A 20:80 output coupler (OC) is used to lock the pulse output while ensuring that most of the energy remains in the cavity. The dispersion values of the SMF-28e, TH512, and SM1950 fibers are −0.0670 ps^2/m, −0.0730 ps^2/m (Tang et al., 2015), and −0.0732 ps^2/m at 1950 nm, respectively. The total dispersion value and cavity length are −1.048 ps^2 and 14.6 m, respectively. An optical spectrum analyzer (AQ6370C, YOKOGAWA, Japan), a 12.5 GHz InGaAs photodetector (ET-5000, EOT, America), a 1 GHz digital storage oscilloscope (DSO9104A, Agilent, America), a radio frequency (RF) spectrum analyzer (N9320B, Agilent, America), and an optical intensity autocorrelator (FR-103HS, Femtochrome, America) are used to monitor the properties of the pulse outputs from the 20% port of the OC.
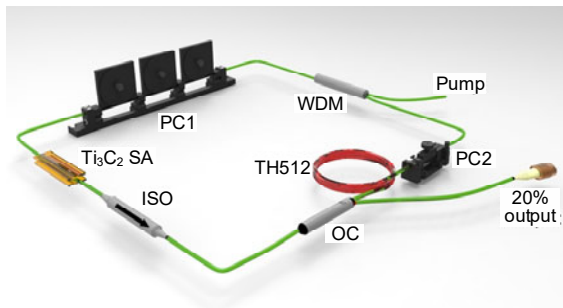

Fig. 4 Schematic of the fiber laser
WDM: wavelength division multiplexer; PC: polarization controller; ISO: isolator; OC: output coupler; TH512: Thulium/Holmium-doped fiber; Ti_3C_2 SA: side-polished D-shaped fiber Ti_3C_2 saturable absorber

4 Experimental results and analysis

4.1 Vector solitons

In our experiments, various mode-locking states were obtained by carefully adjusting the pump power and the polarization controller. When the pump power reached 1.13 W, the mode-locking pulse could be obtained in the laser cavity. As shown in Fig. 5a, the 3 dB spectral bandwidth of the optical spectrum of the mode-locked pulse is 4 nm. The central wavelength is 1965 nm, and there exist two sets of Kelly sidebands, which is the sign of a typical vector soliton (Song et al., 2012, 2019b). There are several continuous wave (CW) spikes on the top of the spectrum, close to the center. It is difficult to compress them. Fig. 5b shows the measured oscilloscope traces. It is a state of harmonic mode-locking on the order of 19. There are certain CWs existing in the background. Fig. 5c is the RF spectrum of the total output. It can be seen that the side mode compression is about 60 dB. Note that the closest side mode is not the fundamental repetition frequency, which should be at the separation at about 13.7 MHz. It is caused by the unstable dispersive waves in the fiber laser (Zhao et al., 2005). The first RF order is about 260.7 MHz, which corresponds to the 19th harmonic mode-locking and matches the oscilloscope measurement. Apart from the 19th order, other orders of harmonic mode-locking
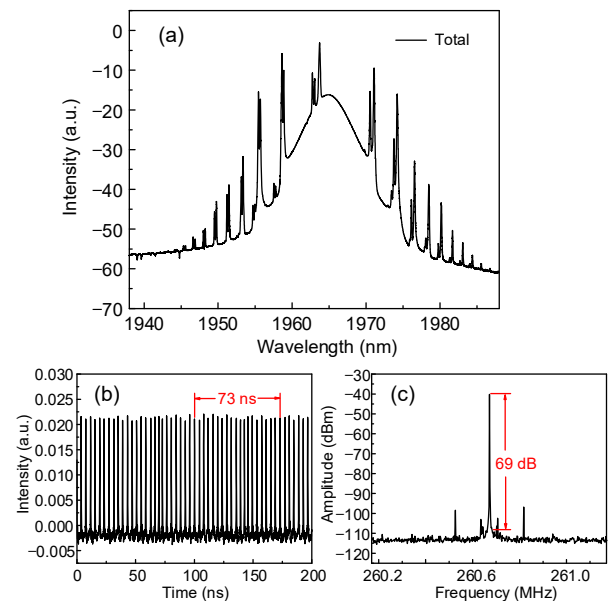

Fig. 5 Vector soliton operation: (a) spectrum of the vector soliton; (b) corresponding mode-locked pulse train; (c) RF spectrum

were also obtained (Yin et al., 2015), but with less stability.

To explore the vector characteristics, we used a polarization beam splitter (PBS) and a polarization controller at the output of the cavity to resolve the output into two beams whose polarizations were orthogonal to each other. By carefully adjusting the polarization controller outside the cavity to compensate for the birefringence of the external fiber pigtails, we obtained the results (Fig. 6). It can be seen that there is only one set of Kelly sidebands on the corresponding spectrum for either the horizontal or vertical polarization component in Fig. 6a. Figs. 6b and 6c are the corresponding RF diagrams of the two polarization directions. It can be seen that the signal-to-noise ratio (SNR) of the output light in the vertical polarization axis is 12 dB higher than that in
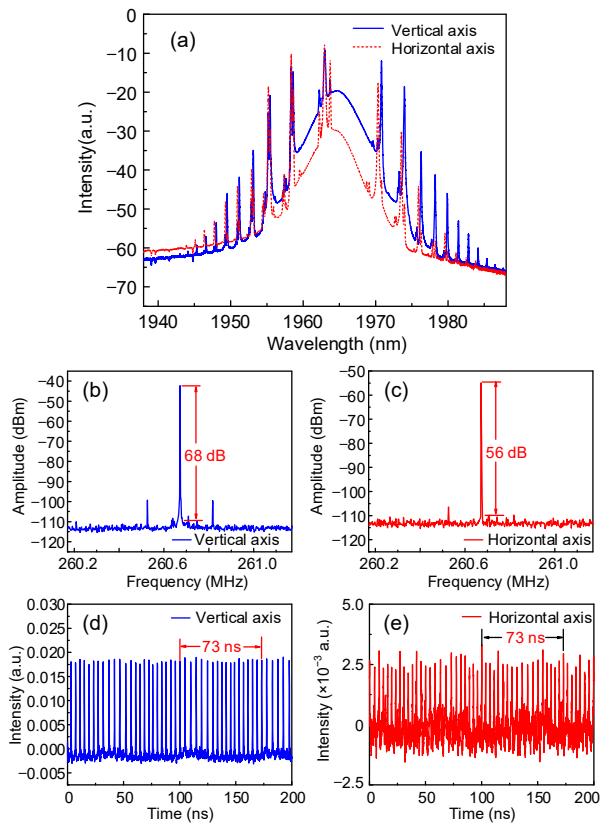

Fig. 6 Vector soliton operation after splitting of the polarization beam splitter (PBS): (a) corresponding spectrum diagram of the horizontal and vertical polarization axes; (b) RF spectrum of the vertical polarization axis; (c) RF spectrum of the horizontal polarization axis; (d) mode-locked pulse train of the vertical polarization axis; (e) mode-locked pulse train of the horizontal polarization axis

the horizontal axis. Figs. 6d and 6e are the time-domain pulse trains, and the signal in the horizontal polarization component is also obviously lower in intensity and unstable. However, it can be seen from both of the RF spectrums and the time-domain pulse trains that both polarization axes correspond to the 19th-order harmonic mode-locked state.

Comparison experiments were carried out, where the MXene SA was replaced with an uncoated D-shaped fiber. No mode-locking was achieved. Therefore, the mode-locking is caused mainly by the MXene SA rather than the polarization-dependent loss related to the D-shaped fiber. Consequently, vector soliton pulse generation is supported.

4.2 Noise-like pulses

Careful adjustment of the polarization controller can gradually transform the VSs into NLPs while keeping the pump power constant. Fig. 7a shows a typical state for NLPs with a 3 dB spectral bandwidth of about 3.3 nm. Figs. 7b and 7c are the corresponding pulse train and RF spectrum, respectively. The SNR of the RF spectrum is 56 dB. During the polarization adjustment, the CW peak remained at 1964 nm while the sideband structures became blurred.

Different from other fiber lasers, the fiber laser here could not be self-started. We suspect that the large insertion loss of the SA might be the reason. The harmonic mode-locking state was always obtained after mode-locking was achieved by tuning the polarization controller. The harmonic order of the VSs depends on the pump power setting. Experimentally, it is difficult to remove the CW components by manipulating the polarization controller and controlling the pump power. After obtaining the harmonic mode-locking state, reducing the pump power could not reduce the harmonic order due to the elimination of the mode-locking state. Re-adjustment of the polarization controller was required to achieve mode-locking again.

As is generally known, an NLP is generally formed by the collapse of solitons. This is undesirable in ultrafast mode-locked fiber lasers that have a narrow bandwidth and high repetition. It has been reported that the use of a topological insulator (TI) Bi_2Se_3 grown by high-quality molecular beam epitaxy (MBE) as a SA can obtain a stable soliton mode-locked laser output without an NLP in a fiber

laser (Miao et al., 2019). Recently, there has been considerable research on other new 2D materials (Zhang J et al., 2018; Zhang CX et al., 2019). Therefore, TIs based on various new 2D materials including the MXenes are expected to be used as SAs to achieve higher-quality mode-locking.
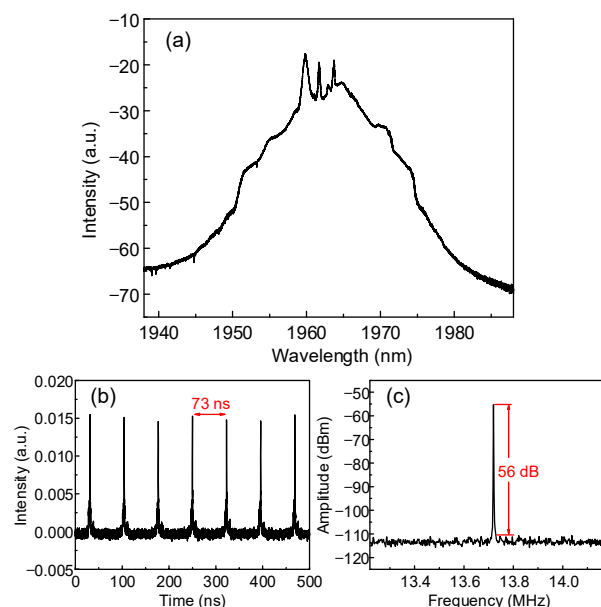

Fig. 7 Noise-like pulse operation: (a) spectrum of the vector soliton; (b) corresponding mode-locked pulse train; (c) RF spectrum

5 Conclusions

In this work, we experimentally obtained VSs and NLPs using a Ti_3C_2 MXene based SA in a Tm:Ho co-doped fiber laser. There are no polarization-dependent components in the cavity. The VSs that we obtained are a 19th harmonic mode-locking pulse train with a center wavelength of 1965 nm and a 3 dB bandwidth of 4 nm. By properly adjusting the polarizations in the cavity, the VSs could evolve into NLPs with a 3 dB bandwidth of 3.3 nm. Our results demonstrated for the first time that a Ti_3C_2 MXene can be used as a polarization-independent SA in fiber lasers, and this paves the way for the study of vector features in mode-locked fiber lasers.

Contributors

Shuai WANG designed the research, processed the data, and drafted the manuscript. Lei LI contributed to the experiments with laser setup and data collection. Yu-feng SONG

provided the SAs. Ding-yuan TANG and De-yuan SHEN coordinated the collaboration. Lu-ming ZHAO helped organize the manuscript. Shuai WANG and Lu-ming ZHAO revised and finalized the paper.

Compliance with ethics guidelines

Shuai WANG, Lei LI, Yu-feng SONG, Ding-yuan TANG, De-yuan SHEN, and Lu-ming ZHAO declare that they have no conflict of interest.

References

Chen Y, Jiang GB, Chen SQ, et al., 2015. Mechanically exfoliated black phosphorus as a new saturable absorber for both Q-switching and mode-locking laser operation. *Opt Expr*, 23(10):12823-12833.
https://doi.org/10.1364/OE.23.012823

Feng XY, Ding BY, Liang WY, et al., 2018. MXene $Ti_3C_2T_x$ absorber for a 1.06 μm passively Q-switched ceramic laser. *Laser Phys Lett*, 15(8):085805.
https://doi.org/10.1088/1612-202X/aac91d

Hantanasirisakul K, Zhao MQ, Urbankowski P, et al., 2016. Fabrication of $Ti_3C_2T_x$ MXene transparent thin films with tunable optoelectronic properties. *Adv Electron Mater*, 2(6):1600050. https://doi.org/10.1002/aelm.201600050

Jiang Q, Zhang M, Zhang Q, et al., 2019. Thulium-doped mode-locked fiber laser with MXene saturable absorber. Conf on Lasers and Electro-Optics, Article SF3O.3.
https://doi.org/10.1364/CLEO_SI.2019.SF3O.3

Jiang T, Yin K, Wang C, et al., 2020. Ultrafast fiber lasers mode-locked by two-dimensional materials: review and prospect. *Photon Res*, 8(1):78-90.
https://doi.org/10.1364/PRJ.8.000078

Lei JC, Zhang X, Zhou Z, 2015. Recent advances in MXene: preparation, properties, and applications. *Front Phys*, 10(3):276-286.
https://doi.org/10.1007/s11467-015-0493-x

Li J, Zhang ZL, Du L, et al., 2019. Highly stable femtosecond pulse generation from a MXene $Ti_3C_2T_x$ (T=F, O, or OH) mode-locked fiber laser. *Photon Res*, 7(3):260-264.
https://doi.org/10.1364/PRJ.7.000260

Lu J, Zou X, Li C, et al., 2017. Picosecond pulse generation in a mono-layer MoS_2 mode-locked Ytterbium-doped thin disk laser. *Chin Opt Lett*, 15(4):041401.

Luo ZQ, Zhou M, Weng J, et al., 2010. Graphene-based passively Q-switched dual-wavelength erbium-doped fiber laser. *Opt Lett*, 35(21):3709-3711.
https://doi.org/10.1364/OL.35.003709

Miao RL, Tong MY, Yin K, et al., 2019. Soliton mode-locked fiber laser with high-quality MBE-grown Bi_2Se_3 film. *Chin Opt Lett*, 17(7):071403.
https://doi.org/10.3788/COL201917.071403

Naguib M, Kurtoglu M, Presser V, et al., 2011. Two-dimensional nanocrystals produced by exfoliation of Ti_3AlC_2. *Adv Mater*, 23(37):4248-4253.
https://doi.org/10.1002/adma.201102306

Nicholson JW, Windeler RS, DiGiovanni DJ, 2007. Optically

driven deposition of single-walled carbon-nanotube saturable absorbers on optical fiber end-faces. *Opt Expr*, 15(15):9176-9183.
https://doi.org/10.1364/OE.15.009176

Qin ZP, Xie GQ, Zhang H, et al., 2015. Black phosphorus as saturable absorber for the Q-switched Er:ZBLAN fiber laser at 2.8 μm. *Opt Expr*, 23(19):24713-24718.
https://doi.org/10.1364/OE.23.024713

Scholle K, Lamrini S, Koopmann P, et al., 2010. 2 μm laser sources and their possible applications. In: Pal B (Ed.), Frontiers in Guided Wave Optics and Optoelectronics. InTech, Vukovar, p.471-500.
https://doi.org/10.5772/39538

Shi W, Fang Q, Zhu XS, et al., 2014. Fiber lasers and their applications [invited]. *Appl Opt*, 53(28):6554-6568.
https://doi.org/10.1364/AO.53.006554

Song YF, Zhang H, Tang DY, et al., 2012. Polarization rotation vector solitons in a graphene mode-locked fiber laser. *Opt Expr*, 20(24):27283-27289.
https://doi.org/10.1364/OE.20.027283

Song YF, Chen S, Zhang Q, et al., 2016. Vector soliton fiber laser passively mode locked by few layer black phosphorus-based optical saturable absorber. *Opt Expr*, 24(23):25933-25942.
https://doi.org/10.1364/OE.24.025933

Song YF, Chen YX, Jiang XT, et al., 2019a. Nonlinear few-layer MXene-assisted all-optical wavelength conversion at telecommunication band. *Adv Opt Mater*, 7(18):1801777. https://doi.org/10.1002/adom.201801777

Song YF, Shi XJ, Wu CF, et al., 2019b. Recent progress of study on optical solitons in fiber lasers. *Appl Phys Rev*, 6(2):021313. https://doi.org/10.1063/1.5091811

Sotor J, Sobon G, Kowalczyk M, et al., 2015. Ultrafast thulium-doped fiber laser mode locked with black phosphorus. *Opt Lett*, 40(16):3885-3888.
https://doi.org/10.1364/OL.40.003885

Tang YX, Chong A, Wise FW, 2015. Generation of 8 nJ pulses from a normal-dispersion thulium fiber laser. *Opt Lett*, 40(10):2361-2364.
https://doi.org/10.1364/OL.40.002361

Wang C, Peng QQ, Fan XW, et al., 2018. MXene Ti$_3$C$_2$T$_x$ saturable absorber for pulsed laser at 1.3 μm. *Chin Phys B*, 27(9):094214.
https://doi.org/10.1088/1674-1056/27/9/094214

Wang C, Wang YZ, Jiang XT, et al., 2019. MXene Ti$_3$C$_2$T$_x$: a promising photothermal conversion material and application in all-optical modulation and all-optical information loading. *Adv Opt Mater*, 7(12):1900060.
https://doi.org/10.1002/adom.201900060

Yin K, Zhang B, Li L, et al., 2015. Soliton mode-locked fiber laser based on topological insulator Bi$_2$Te$_3$ nanosheets at 2 μm. *Photon Res*, 3(3):72-76.
https://doi.org/10.1364/PRJ.3.000072

Zhang CX, Ouyang H, Miao RL, et al., 2019. Anisotropic nonlinear optical properties of a SnSe flake and a novel perspective for the application of all-optical switching. *Adv Opt Mater*, 7(18):1900631.
https://doi.org/10.1002/adom.201900631

Zhang H, Tang DY, Zhao LM, et al., 2009. Large energy mode locking of an erbium-doped fiber laser with atomic layer graphene. *Opt Expr*, 17(20):17630-17635.
https://doi.org/10.1364/OE.17.017630

Zhang H, Tang DY, Knize RJ, et al., 2010. Graphene mode locked, wavelength-tunable, dissipative soliton fiber laser. *Appl Phys Lett*, 96(11):111112.
https://doi.org/10.1063/1.3367743

Zhang J, Jiang T, Zhou T, et al., 2018. Saturated absorption of different layered Bi$_2$Se$_3$ films in the resonance zone. *Photon Res*, 6(10):C8-C14.
https://doi.org/10.1364/PRJ.6.0000C8

Zhao B, Tang DY, Kong J, et al., 2005. Periodic soliton amplitude variation caused by unstable dispersive waves in a laser. *Opt Commun*, 254(4-6):242-247.
https://doi.org/10.1016/j.optcom.2005.05.055

Zu YQ, Zhang C, Guo XS, et al., 2019. A solid-state passively Q-switched Tm,Gd:CaF$_2$ laser with a Ti$_3$C$_2$T$_x$ MXene absorber near 2 μm. *Laser Phys Lett*, 16(1):015803.
https://doi.org/10.1088/1612-202X/aaef99